8756 *Biochemistry* **2010,** *49,* 8756–8765
DOI: 10.1021/bi1008613

BIOCHEMISTRY
including biophysical chemistry & molecular biology
Article

Molecular Details of the Yeast Frataxin−Isu1 Interaction during Mitochondrial Fe−S Cluster Assembly[†]

Jeremy D. Cook,[‡] Kalyan C. Kondapalli,[‡] Swati Rawat,[‡] William C. Childs,[‡] Yogapriya Murugesan,[‡] Andrew Dancis,[§] and Timothy L. Stemmler*[,‡]

[‡]*Department of Biochemistry and Molecular Biology, Wayne State University, School of Medicine, Detroit, Michigan 48201, and* [§]*Department of Medicine, Division of Hematology-Oncology, University of Pennsylvania, Philadelphia, Pennsylvania 19104*

Received June 1, 2010; Revised Manuscript Received September 3, 2010

ABSTRACT: Frataxin, a conserved nuclear-encoded mitochondrial protein, plays a direct role in iron−sulfur cluster biosynthesis within the ISC assembly pathway. Humans with frataxin deficiency have Friedreich's ataxia, a neurodegenerative disorder characterized by mitochondrial iron overload and disruption in Fe−S cluster synthesis. Biochemical and genetic studies have shown frataxin interacts with the iron−sulfur cluster assembly scaffold protein (in yeast, there are two, Isu1 and Isu2), indicating frataxin plays a direct role in cluster assembly, possibly by serving as an iron chaperone in the assembly pathway. Here we provide molecular details of how yeast frataxin (Yfh1) interacts with Isu1 as a structural module to improve our understanding of the multiprotein complex assembly that completes Fe−S cluster assembly; this complex also includes the cysteine desulfurase (Nfs1 in yeast) and the accessory protein (Isd11), together in the mitochondria. Thermodynamic binding parameters for protein partner and iron binding were measured for the yeast orthologs using isothermal titration calorimetry. Nuclear magnetic resonance spectroscopy was used to provide the molecular details to understand how Yfh1 interacts with Isu1. X-ray absorption studies were used to electronically and structurally characterize how iron is transferred to Isu1 and then incorporated into an Fe−S cluster. These results were combined with previously published data to generate a structural model for how the Fe−S cluster protein assembly complex can come together to accomplish Fe−S cluster assembly.

Iron−sulfur (Fe−S) clusters are central to life and found in nearly every class of organism (*1*). These ancient but conserved cofactors are bound to proteins involved in a diverse array of essential functions, ranging from DNA repair to respiration. Because Fe−S cofactors are essential for cell viability, it is no surprise that proteins producing these cofactors are tightly controlled and evolutionarily conserved (*2*−*4*). In eukaryotes, the major Fe−S cluster assembly machinery is found in the mitochondria. The process of Fe−S cluster synthesis involves the formation of an Fe−S cluster intermediate on a scaffold protein (ISCU in humans or Isu1 or Isu2 in yeast) and subsequent transfer of the cluster to recipient apoproteins. Formation of the Fe−S cluster by Isu1 requires a source of sulfur and a source of iron. The sulfur originates from cysteine via the activity of the cysteine desulfurase Nfs1, which is coordinated with the essential accessory protein Isd11. The source of the iron for Fe−S clusters has remained a mystery. Frataxin (Yfh1 in yeast), a small acidic mitochondrial protein, is directly linked to cluster assembly and has been suggested to serve as an iron chaperone through formation of a complex with Isu1, Nfs1, and Isd11 (*5*−*8*).

Humans with frataxin deficiency have the cardiodegenerative and neurodegenerative disorder Friedreich's ataxia (FRDA) (*9*−*11*). FRDA affects 1 in 50,000 live births, and the disorder is caused in ∼98% of the cases by a transcription disrupting trinucleotide repeat expansion in the first intron of the frataxin gene leading to decreased transcription and protein levels (*9*). Frataxin is essential for cellular iron homeostasis, and deficiency is associated with mitochondrial iron overload, low heme and Fe−S cluster production levels, and higher formation of reactive oxygen species (*12*). Numerous reports have shown direct interactions between frataxin and the scaffold protein in mitochondrial lysates or through isolation (*5*, *6*, *8*, *13*). In addition, frataxin has been shown to facilitate assembly of the Fe−S cluster intermediate on Isu1 (*14*−*16*). Combined, these data strongly suggest that frataxin plays a direct role in Fe−S cluster bioassembly, possibly by serving as the iron chaperone or, as recently suggested (*14*), as a regulator within the assembly pathway.

Participation of frataxin in the Fe−S cluster assembly pathway is directly correlated to the protein's ability to bind iron, and this metal binding ability has been studied extensively for the different frataxin orthologs. Yeast frataxin was the first to exhibit iron binding ability (*17*). When placed in an oxygen-rich, low-salt, high-iron:protein ratio environment, the protein forms oligomers that retain metal as ferrihydrite in a manner that resembles the activity of ferritin (*17*). This ability has been shown to be important under oxidative stress conditions (*18*). However, frataxin mutations that disrupt oligomerization are functionally competent in promoting Fe−S cluster assembly in vivo, even when produced at low levels; thus, oligomerization is not required for the physiological function of frataxin in the assembly of Fe−S clusters (*8*, *19*). As a monomer, the different frataxin orthologs bind iron with micromolar binding affinities (*15*, *16*, *20*−*24*). Frataxin binding to the scaffold protein is independent of frataxin aggregation but dependent on the presence of iron (*8*, *15*). It is therefore of direct physiological interest to explore the molecular details of the interaction between frataxin and the

[†]This work was supported by the American Heart Association (Grant 0610139Z to K.C.K.) and the National Institutes of Health (Grant DK53953 to A.D. and Grant DK068139 to T.L.S.).

*To whom correspondence should be addressed: Department of Biochemistry and Molecular Biology, Wayne State University, School of Medicine, 540 E. Canfield Ave., Detroit, MI 48201. Telephone: (313) 577-5712. Fax: (313) 577-2765. E-mail: tstemmle@med.wayne.edu.

 Published on Web 09/03/2010

scaffold protein to improve our understanding of the functional details of the cofactor assembly pathway.

In this report, we provide new molecular details that are pivotal for understanding the interaction between Yfh1 and Isu1. We probe the nature of holo-Yfh1 binding to Isu1 using isothermal titration calorimetry (ITC).[1] Nuclear magnetic resonance spectroscopy was used to map the intermolecular interface where Isu1 binds on Yfh1 to help identify frataxin residues that participate in the formation of the multiprotein complex. X-ray absorption spectroscopy was used to determine the electronic and structural properties of iron at multiple stages during Fe−S cluster assembly on the Isu1 scaffold. Finally, the fold of Isu1 was characterized at different stages during Fe−S cluster assembly using fluorescence spectroscopy. These combined results provide molecular details that are essential to understanding mitochondrial Fe−S cluster assembly.

EXPERIMENTAL PROCEDURES

Molecular Biology and Protein Purification. The plasmid for expression of mature Isu1 (without 35 amino-terminal amino acids) containing the D37A mutation (known to prevent release of the Fe−S cluster from the protein) and the biophysical characterization of the apoprotein was described previously (*15*). Briefly, the plasmid was transformed into BL21(DE3) CodonPlus cells and grown by autoinduction (*25*) at 25 °C for ∼24 h before the cells were harvested by centrifugation. Protein isolation steps were all performed at 4 °C. Cells were resuspended in 50 mM $NaPO_4$ (pH 7.5), 300 mM NaCl, 20 mM imidazole, and 5 mM β-Me (5 mL/g of cells) in the presence of Complete EDTA free protease inhibitor cocktail (Roche), lysed by two passes through a French pressure cell followed by two rounds of sonication (50% power for 20 s), and centrifuged at high speed (21,000 rpm) for 1 h. The crude soluble fraction was filtered (0.20 μm) and loaded onto a HisPrep FF Ni column (Pharmacia) using an imidazole gradient (from 20 to 500 mM; protein elutes at ∼120 mM). Isu1-containing fractions were pooled and concentrated to ∼1 mL using 3 kDa cutoff centricons (Millipore) and run over a Sephadex 75 size exclusion column (Pharmacia) equilibrated with 20 mM HEPES buffer (pH 7.5), 150 mM NaCl, and 5 mM β-Me. The protein eluted at a volume consistent with a 15.5 kDa size, and we were able to attain ≥95% pure protein based on gel analysis (typical yields were 15 mg/L).

Apo-Yfh1 was isolated as described previously (*22*). Briefly, wild-type Yfh1 was subcloned into a pET11a expression vector (Novagen), transfected into BL21(DE3) cells, and grown via autoinduction (*25*) at 37 °C for 18 h before the cells were harvested via centrifugation. All subsequent steps were performed at 4 °C. Cells were resuspended in 25 mM Tris buffer (pH 8.0), 10 mM EDTA, and 5 mM β-Me with Complete protease inhibitor cocktail, lysed using two passes through a French pressure cell followed by two rounds of sonication at 50% power, and spun at high speed (21,000 rpm for 1 h). A 30% ammonium sulfate (AS) condition was applied to the supernatant and spun down (8000 rpm for 10 min). The remaining supernatant was brought to 65% AS and again spun down (8000 rpm for 10 min). The pellet was then resuspended in a minimal volume of 25 mM Tris (pH 8.0), 10 mM EDTA, 5 mM β-Me, and one protease inhibitor tablet, set to stir for 20 min before being loaded into a dialysis membrane (10 kDa cutoff), and dialyzed into the same buffer overnight with one buffer change. The resultant protein mixture was filtered twice (0.45 and 0.20 μm) before being loaded onto a Q-Sepharose anion exchange column (Pharmacia) equilibrated with 25 mM Tris buffer (pH 8.0), 10 mM EDTA, and 5 mM β-Me and run with a linear salt gradient (from 0 to 1 M NaCl; protein elutes at ∼0.5 M salt). Active fractions were confirmed by sodium sulfate dodecyl−polyacrylamide gel electrophoresis (SDS−PAGE) analysis and pooled with protease inhibitor before being desalted by dialysis against 25 mM Tris buffer (pH 8.0), 10 mM EDTA, and 5 mM β-Me overnight with one buffer change. Protein was brought up to 1 M ammonium sulfate (Sigma), filtered twice (0.45 μm, 0.20 μm), and loaded onto a Phenyl-Sepharose column equilibrated with 25 mM Tris buffer (pH 8.0), 10 mM EDTA, 5 mM β-Me, and 1 M ammonium sulfate and run with a reverse ammonium sulfate linear gradient (protein elutes at ∼0.8 M salt). Active fractions were pooled and dialyzed overnight into 20 mM HEPES buffer (pH 7.5), 150 mM NaCl, and 5 mM β-Me and concentrated using 10 kDa cutoff centricons (Millipore) for a typical yield of 60 mg/L.

Isothermal Titration Calorimetry. ITC measurements were performed to determine the binding affinity and stoichiometry among monomeric yeast frataxin, ferrous iron, and/or Isu1. Experiments were performed anaerobically at 30 °C on a VP-ITC titration microcalorimeter (MicroCal Inc.). ITC experiments were performed for Yfh1 and Fe, Yfh1 and Isu1, and holo-Yfh1 and Isu1, with an iron:frataxin stoichiometric ratio of 1:1. Holo-Yfh1 samples were prepared anaerobically under solution conditions that stabilize the protein as a monomer [20 mM HEPES (pH 7.5), 150 mM NaCl, and 5 mM β-Me] in the same manner previously described (*21*); the monomeric state was verified using size-exclusion chromatography (data not shown). Experiments contained 30 μM protein in the adiabatic cell and 500 μM titrant in the syringe. After an initial 2 μL injection, 29 additional injections of 10 μL were spaced out by 10 min each with constant stirring (500 rpm). All protein/metal buffers were matched by dialysis before being loaded into the ITC instrument. Protein samples were extensively degassed, and buffers were purged with Ar(g) before data were collected to maintain and stabilize the ferrous iron. Spectra were recorded for duplicate and triplicate independent sample sets. Data were fit and analyzed using Origin version 5.0 supplied by MicroCal (GE Life Sciences), which uses a nonlinear least-squares curve fitting algorithm to determine the stoichiometric ratio, dissociation constant, and change in enthalpy of the reaction.

Nuclear Magnetic Resonance Spectroscopy. ^{15}N-labeled Yfh1 was isolated from *Escherichia coli* transfected with the Yfh1 plasmid, grown in M9 minimal medium supplemented with [^{15}N]NH_4Cl at 37 °C for 4 h after induction with 1 mM IPTG, and isolated as described above. ^{1}H−^{15}N TROSY heteronuclear single-quantum coherence (HSQC) data were collected on a Varian INOVA 600 MHz spectrometer equipped with a triple-resonance ^{1}H, ^{13}C, ^{15}N Varian cold probe with *z*-axis pulsed field gradients (*26*). Titrations were performed in septa-sealed NMR tubes under anaerobic conditions using two independent buffer conditions: (1) 25 mM $NaPO_4$ buffer (pH 7.5) with 2 mM DTT buffer and (2) 20 mM HEPES buffer (pH 7.5), 150 mM NaCl, and 5 mM β-Me. The ^{15}N-labeled Yfh1 concentration was ∼200 μM after addition of 1 equivalent of ferrous iron and 1 equivalent of Isu1 dimer. Data were collected for apo-Yfh1, holo-Yfh1, and apo-Yfh1−Isu1 and holo-Yfh1−Isu1 complex samples. Protein samples were placed in the NMR spectrometer and allowed to equilibrate at 30 °C for 30 min prior to sample collection. Full ^{1}H−^{15}N TROSY-HSQC spectra were recorded with a ^{1}H sweep width of 7804 Hz (2048 points and 64 transients) and at a ^{15}N sweep width of

[1]Abbreviations: NMR, nuclear magnetic resonance; XAS, X-ray absorption spectroscopy; XANES, X-ray absorption near edge structure; EXAFS, extended X-ray absorption fine structure; ITC, isothermal titration calorimetry; ANS, 1,8-anilinonaphthalene sulfonate.

2500 Hz (512 increments). Spectra were referenced using a DSS standard and transformed using NMRPipe (*27*), and peak positions were calculated using SPARKY (*28*). Normalized chemical shifts were calculated using the published peaks files following the equation $\delta = 25[(\delta_{HN})^2 + (\delta_N/5)^2]^{0.5}$. Results presented in Figure 2B represent the average of both experiments. Residues that underwent significant chemical shift perturbations were identified using MOLMOL in Figure 2C on the apo-yeast frataxin solution structure [Protein Data Bank (PDB) entry 2GA5].

X-ray Absorption Spectroscopy. X-ray absorption spectroscopy was used to study the electronic properties and ligand coordination geometry of iron at different stages during Fe−S cluster assembly. All samples were prepared anaerobically within a glovebox (PlasLabs) using protein and iron solutions that were initially degassed on a Schlenk line and stored under an Ar(g) atmosphere. XAS samples were prepared at final protein concentrations of ~0.5 mM in 20 mM HEPES buffer (pH 7.0), 150 mM NaCl, and 5 mM β-Me. The individual samples prepared were as follows: (1) Isu1 incubated with 0.95 equiv of ferrous iron, (2) Yfh1 incubated with 0.95 equiv of ferrous iron for 10 min at room temperature before addition of Isu1, (3) Isu1 incubated with 0.95 equiv of ferrous iron for 10 min at room temperature before addition of 1 equiv of Na_2S, and (4) Yfh1 incubated with 0.95 equiv of iron for 10 min at room temperature before addition of Isu1 and 1 equiv of Na_2S. All samples were allowed to incubate for an additional 60 min in an Ar(g) atmosphere to ensure cluster and complex formation. Samples were diluted with 30% glycerol as a glassing agent, loaded into Lucite sample cells wrapped with Kapton tape, flash-frozen in liquid nitrogen, removed from the glovebox, and stored in liquid nitrogen until data collection was performed.

XAS data were collected at the Stanford Synchrotron Radiation Laboratory (SSRL), beamlines 7-3 and 9-3, and at the National Synchrotron Light Source (NSLS), beamline X3-b. SSRL beamline 7-3 was equipped with a single rhodium-coated silicon mirror and a Si[220] double-crystal monochromator, and harmonic rejection was achieved by detuning the monochromator 50%. SSRL beamline 9-3 was equipped with a Si[220] double-crystal monochromator and a harmonic rejection mirror, so spectra were collected under fully tuned conditions. NSLS beamline X-3b used a Si[111] single-crystal monochromator equipped with a nickel-coated cylindrically bent mirror to achieve harmonic rejection and vertical focusing. Samples were maintained at 10 K using Oxford Instrument continuous-flow liquid helium cryostats at SSRL locations and at ca. 24 K using a He Displex Cryostat at NSLS. Protein fluorescence excitation spectra were recorded using 30-element Ge solid-state array detectors at SSRL locations and a 13-element Ge solid-state detector at NSLS. XAS spectra were recorded using 5 eV steps in the pre-edge regions (6900−7094 eV), 0.25 eV steps in the edge regions (7095−7135 eV), and 0.05 Å^{-1} increments in the extended X-ray absorption fine structure (EXAFS) region (to k = 13.5 Å^{-1}), integrating from 1 to 20 s in a k^3-weighted manner for a total scan length of approximately 40 min. X-ray energies were calibrated via simultaneous collection of an iron foil absorption spectrum and collection of protein data. The first inflection point for the Fe foil edge was assigned at 7111.3 eV. Each fluorescence channel of each scan was examined for spectral anomalies prior to averaging, and spectra were closely monitored for photoreduction. SSRL protein data represent the average of five to six scans, while NSLS protein data represent the average of eight to nine scans.

XAS data were processed using the Macintosh OS X version of the EXAFSPAK program suite (*29*) integrated with Feff version 7.2 for theoretical model generation. XAS data reduction utilized a Gaussian function in the pre-edge region and a three-region cubic spline in the EXAFS region. EXAFS data were converted to k space using an E_0 value of 7130 eV. The k^3-weighted EXAFS was truncated at 1.0 and 13.0 Å^{-1} for filtering purposes and Fourier transformed. The final fitting results listed in Table 3 are from averaged values obtained from simulations of raw unfiltered data. Edge inflection energies were calculated as the maximum of the first derivative of the XANES spectra. Analysis of the XANES 1s → 3d transitions was completed using the EDG_FIT subroutine within EXAFSPAK. Only spectra collected using the higher-resolution Si[220] monochromator crystals were subjected to edge analysis. Pre- and postedge splines were fit to the experimental spectra within the energy ranges of 7090−7100 and 7120−7125 eV, respectively. The extrapolated line was then subtracted from raw data to yield baseline-corrected spectra. Pre-edge features were modeled using pseudo-Voigt line shapes (simple sums of Lorentzian and Gaussian functions), and the energy position, the full width at half-maximum (fwhm), and the peak heights for each transition were varied. A fixed 50:50 ratio of Lorentzian to Gaussian functions successfully reproduced the spectral features of the pre-edge transitions. Global peak transition areas were determined for all spectra over the energy range of 7109−7117 eV using Kaleidagraph. Pre-edge intensity values were calibrated by multiplying values by 100.

EXAFS data fitting analysis performed on both Fourier-filtered and raw and unfiltered data gave equivalent structural results. Model and protein EXAFS data were fit using both single- and multiple-scattering amplitude and phase functions calculated using Feff version 7.2. Single-scattering models were calculated for carbon, oxygen, sulfur, and iron coordination to simulate possible iron−ligand environments in our systems (*21*). Fits to crystallographically characterized model compounds were used to calibrate the scale factor and ΔE_0 values. A calibrated scale factor (Sc) of 0.95 and a threshold shift (ΔE_0) of −11.5 eV were used during protein data analysis, and Sc and E_0 were not allowed to vary during the fitting analysis. Simulation protocols and criteria for judging the best fit were outlined previously (*30*).

Fluorescence Spectroscopy. Fluorescence spectroscopy was used to identify structural changes in Isu1 that result from the binding of substrate or following cluster production. The fluorescent dye 1,8-anilinonaphthalene sulfonate (ANS), which selectively binds to solvent-exposed hydrophobic regions found in molten globule proteins, is an effective tool for helping to observe overall changes in the molten globule nature of Isu1 at different states during cluster assembly (*31*). ANS studies were performed using a 3 mL fluorescence cuvette (Starna) equipped with septa, a 50 μM Isu1 solution, in 20 mM HEPES buffer (pH 7.5), 150 mM NaCl, and 5 mM β-Me. Samples and solutions were degassed on a Schlenk line and stored under Ar(g). Independent samples were prepared by incubation of the Isu1 dimer with or without 2 equiv of ferrous iron and/or sulfide. Single-time point fluorescence measurements were taken for protein samples incubated for 10 min before addition of 10 μM ANS followed by a second 10 min incubation before data collection ($\lambda_{excitation}$ = 371 nm, and $\lambda_{emission}$ = 490 nm) on a QuantaMaster fluorimeter (PTI). Data were collected at 1 nm intervals with 0.5 s integration times and 5 mm slit widths. Data were collected in duplicate, and spectra shown in Figure 5 represent a single smoothed spectrum using a window function of five data points. Titration of ANS into Isu1 alone was performed to measure the number of moles of ANS that bind to Isu1 (B_{max}), and the binding affinity was obtained through Scatchard analysis of the variation of bound ANS to protein concentration (*32*).

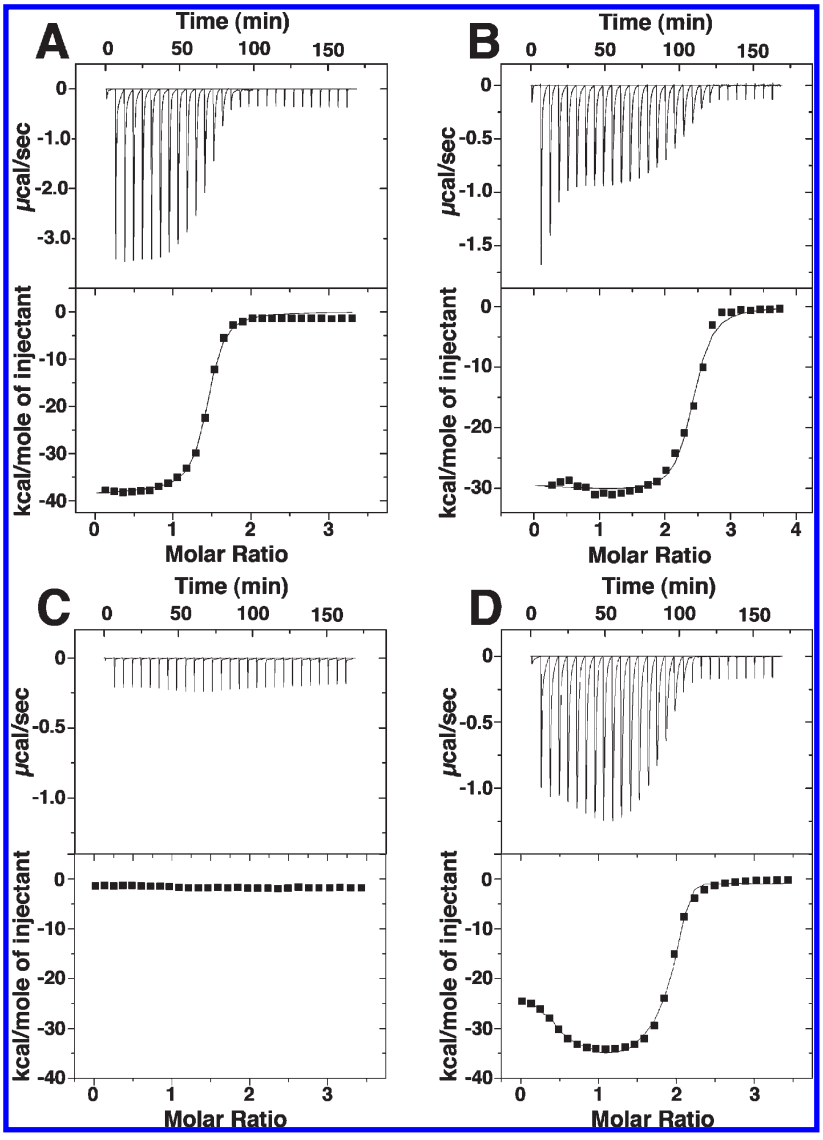

FIGURE 1: Raw isothermal titration calorimetry data (top) and binding isotherm data (bottom) for (A) titration of Fe(II) into Yfh1, (B) titration of Fe(II) into Isu1, (C) titration of Yfh1 into Isu1, and (D) titration of Fe-bound Yfh1 into Isu1. A gray line in each bottom panel shows the simulated fit to the binding isotherm data.

RESULTS

Isothermal Titration Calorimetry. ITC was used to probe the thermodynamic characteristics of the interaction among iron, Yfh1, and Isu1. Our laboratory previously showed monomeric Yfh1 binds two ferrous iron atoms with micromolar binding affinity when millimolar concentrations of $MgSO_4$ were present in the solution buffer (*21*). In our work, we measured the Fe(II) binding affinity and stoichiometry for Yfh1 under solution conditions that stabilize Isu1 [20 mM HEPES (pH 7.5), 150 mM NaCl, and 5 mM β-Me] again using ITC. All data were collected anaerobically in the presence of salt and in duplicate using independently prepared protein samples to promote ferrous iron stability, to prevent protein aggregation, and to test sample reproducibility. Yfh1 exhibited a strong single exothermic binding interaction when binding two iron atoms (Figure 1A), similar to what was observed in our published $MgSO_4$ salt study. Data were best fit using a two-independent site substrate binding model with corresponding K_D values of one Fe(II) atom at 113 ± 2 nM and one Fe(II) atom at 1.64 ± 1.68 μM (Table 1). These affinities are similar but tighter than the average of 3 μM binding affinities observed for the two bound iron atoms in our previous study.

Table 1: Average Simulation Results for ITC Analysis[a]

sample	N_1	K_{D1}	N_2	K_{D2} (nM)
Fe-Yfh1	1.08 ± 0.30	1.64 ± 1.68 μM	1.02 ± 0.38	113 ± 2
Fe-Isu1	1.19 ± 0.66	234 ± 35 nM	0.97 ± 0.31	6 ± 4
Yfh1−Isu1	–	–	–	–
Fe-Yfh1−Isu1	1.67 ± 0.28	166 ± 112 nM	0.52 ± 0.14	5 ± 3

[a]Averaged values of stoichiometry vs the Isu1 monomer (N_1 and N_2) and dissociation constant (K_{D1} and K_{D2}) are given with errors.

ITC was used to measure the energy and stoichiometry of iron with or without Yfh1 binding to apo-Isu1. Aqueous ferrous iron titrated into Isu1 yields a single exothermic binding event (Figure 1B). Heat release data were best simulated using a two-independent substrate binding site model with both iron atoms binding with nanomolar affinity (K_{D1} = 234 ± 35 nM, and K_{D2} = 6 ± 4 nM) per Isu1 monomer (Table 1). Titrations of apo-Yfh1 into apo-Isu1 showed no appreciable heat absorbed or released, indicating the lack of a binding event in the absence of added iron (Figure 1C). However, titration of holo-Yfh1 into Isu1 yielded a strong biphasic exothermic binding event with

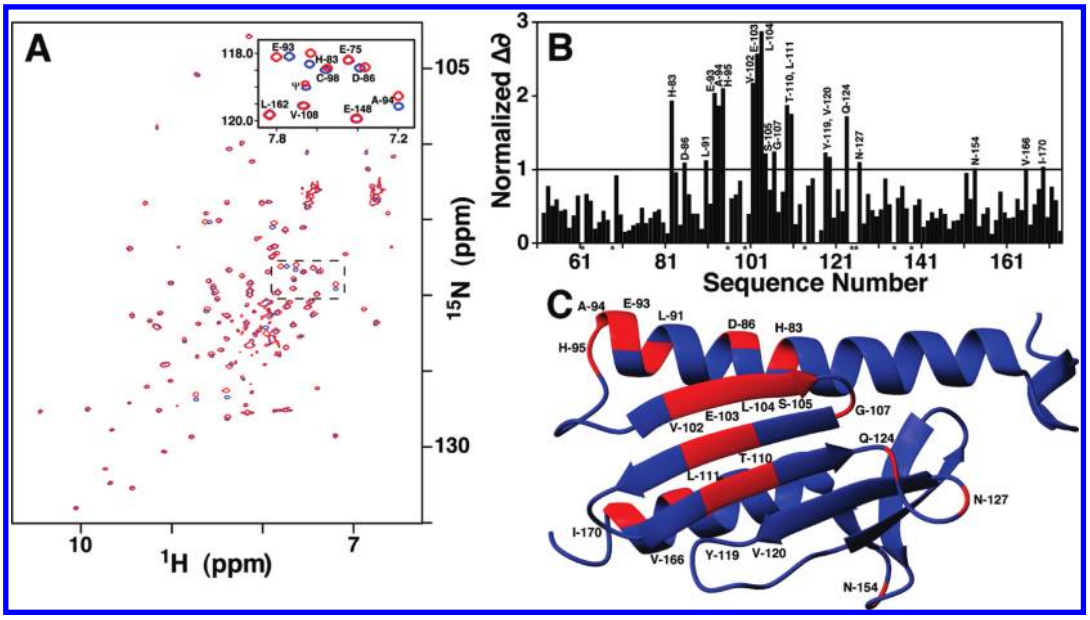

FIGURE 2: NMR chemical shift mapping of Yfh1 residues affected by Isu1 binding. (A) $^{1}H-^{15}N$ HSQC spectra for Fe-Yfh1 in the presence (red) and absence (black) of unlabeled apo-Isu1. Reproducible spectra of the Fe-Yfh1−Isu1 complex were recorded at a 2:1 iron:Yfh1 stoichiometric ratio and a 1:1 Yfh1:Isu1 ratio in phosphate buffer. The region boxed with a dashed line is shown as the inset. (B) Averaged normalized chemical shift changes for Fe-Isu1 with and without Isu1. The line represents the threshold value calculated on the basis of the resolution of the data. (C) Residues identified on the apo-frataxin structure have normalized chemical shift (δ) values of > 1 (colored red).

saturation occurring at approximately 2 equiv of holo-Yfh1 monomer (with one Fe bound) per each Isu1 monomer in the Isu1 protein dimer (Figure 1D). Binding occurred at nanomolar affinities (K_{D1} = 166 ± 112 nM, and K_{D2} = 5 ± 3 nM).

Nuclear Magnetic Resonance Spectroscopy. NMR spectroscopy was used to identify which Yfh1 amino acids reside at the Isu1 binding interface. $^{15}N-^{1}H$ HSQC-TROSY data were collected for apo-Yfh1, holo-Yfh1, the apo-Yfh1−apo-Isu1 complex, and the holo-Yfh1−apo-Isu1 complex. Data were collected under two different buffer conditions: (1) 25 mM $NaPO_4$ (pH 7.5) with 2 mM DTT buffer and (2) 20 mM HEPES (pH 7.5), 150 mM NaCl, and 5 mM β-Me buffer. During the iron titrations, specific Yfh1 amide resonances were observed to change upon addition of iron, as previously reported (*21*, *22*). Titrations under both solution conditions yielded similar results except that data collected in phosphate buffer did not show the amide resonance line broadening effects in the presence of the paramagnetic metal that were observed in the HEPES buffer titration (*21*). Upon further addition of unlabeled apo-Isu1 to labeled holo-Yfh1 (Figure 2A), an additional set of amide resonances underwent a chemical shift perturbation, indicating selective changes in the frataxin amino acid chemical environments caused by Isu1 binding. Normalized chemical shift changes were calculated under both solution conditions, and the averaged normalized chemical shift changes are given in Figure 2B. Only residues with normalized chemical shift changes above the calculated spectral resolution of our data are highlighted in red on the apo-Yfh1 solution structure (Figure 2C). Specific Yfh1 residues affected by the addition of Isu1 comprise portions of both Yfh1 iron-binding sites identified (*21*, *22*) in addition to a major portion of the β-sheet surface of frataxin. Specific residues perturbed by the addition of unlabeled Isu1 to labeled holo-Yfh1 include H83, D86, L91, E93, A94, and H95 (broadly the Yfh1 helix 1 Fe-binding region); V102 and E103 (the Yfh1 strand 1 Fe-binding region); L104, S105, G107, T110, L111, Y119, V120, Q124, and N127 (on the Yfh1 β-sheet surface); and N154, V166, and I170 (on the Yfh1 strand 6−loop and helix 2 region).

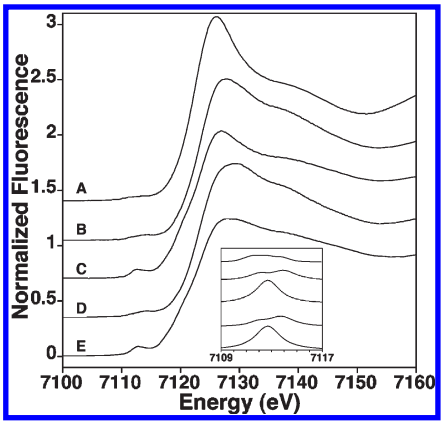

FIGURE 3: Iron XANES spectra of (A) Fe-Yfh1, (B) Fe-Isu1, (C) Fe-Isu1 and S^{2-}, (D) Fe-Yfh1 and Isu1, and (E) Fe-Yfh1, S^{2-}, and Isu1. Individual spectra were equally offset for the sake of clarity. The inset is an expansion of the individual 1s → 3d transition peaks in the same order used in the main panel.

X-ray Absorption Spectroscopy. XANES analyses of the XAS spectra for metal bound to Yfh1 with or without Isu1 with or without S_2^- were examined to characterize the electronic and structural properties of bound iron at different stages of cluster assembly. Complete XAS spectra were recorded for multiple independent versions of the following samples: (A) Fe(II) and apo-Yfh1, (B) Fe(II) and apo-Isu1, (C) Fe(II), S_2^-, and apo-Isu1, (D) Fe-Yfh1 and Isu1, and (E) Fe-Yfh1, S_2^-, and apo-Isu1. XANES spectra of all samples show similar edge features (Figure 3), and the analysis of the first derivative of the edge inflection energies shows values consistent with the bulk iron being stable in the ferrous form (Table 2). Pre-edge 1s → 3d electronic features (i.e., pre-edge energy and absorption area) in the XANES spectra (Figure 3, inset) are consistent with iron, in the samples without sulfide, being six coordinate high-spin Fe(II) with a small shift from octahedral metal−ligand bond symmetry as the samples go from Fe-Yfh1 to Fe-Isu1 to Fe-Yfh1−Isu1. In samples containing sulfide, 1s → 3d pre-edge

transition energies and areas are consistent with a significant portion of the metal being held in a tetrahedral Fe(II)−ligand coordination environment (*33*).

Metric parameters regarding iron ligand identity, iron coordination number (CN), and metal−ligand bond lengths were determined by analysis of the EXAFS portion of the XAS data for the samples listed above. We have previously shown iron bound to Yfh1 (Figure 4A,B) is six-coordinate in a highly symmetric oxygen/nitrogen (O/N) ligand coordination environment, with an average bond length of 2.12 Å (Table 3). Ferrous iron bound to Isu1 (Figure 4C,D) has two unique nearest neighbor ligand coordination environments, both O/N-based with approximately one O/N ligand at 2.01 Å and approximately five O/N ligands centered at 2.14 Å. Interestingly, metal bound to Isu1 alone does not occur via cysteine sulfur ligands, as there is no evidence of sulfur ligation. Long-range scattering in both samples was best fit with carbon scattering at distances ranging from 3.00 to 3.30 Å. Iron, in the Yfh1−Isu1 complex, shows nearest neighbor ligand coordination distinct from that of either Fe-Yfh1 or Fe-Isu1 alone or as a linear combination of both. The nearest neighbor ligand coordination in the Fe-Yfh1−Isu1 sample (Figure 4G,H) consists of two independent environments centered at 1.99 and 2.15 Å; these average bond lengths are consistent with six-coordinate Fe(II)−(O/N) model compounds. While the coordination numbers are similar in both environments (CN values of 2 and 1.5, respectively), the large Debye−Waller factor in the 1.99 Å environment is consistent with significant disorder in this ligand environment producing an abnormally low coordination number for this set of ligands. Long-range scattering in this sample is consistent with multiple carbon-based ligands centered at 3.07, 3.51, and 4.09 Å.

Inclusion of sulfur with the samples described above causes a significant change in the Fe coordination environment. Sulfur added to Isu1 with iron bound (Figure 4E,F) alters the iron nearest neighbor coordination environment so that it includes both O/N and S scattering. The best-fit spectral simulation for the iron coordination includes 2.5 O/N ligands at 2.11 Å, a single sulfur

Table 2: Analysis of Pre-Edge and Edge Features from XANES Spectra Given in Figure 4[a]

sample	pre-edge peak energy (eV)	total pre-edge area	edge inflection energy (eV)
Fe-Yfh1	7111.27 ± 0.02[b]	5.5 ± 0.7[b]	7122.4 ± 0.1[b]
	7112.28 ± 0.03[b]		
	7113.38 ± 0.02[b]		
Fe-Isu1	7111.90 ± 0.14	8.8 ± 0.3	7123.1 ± 0.2
	7113.80 ± 0.28		
Fe-Isu1 and S	7112.63 ± 0.18	22.3 ± 10.0	7123.5 ± 0.2
Fe-Yfh1 and Isu1	7111.70 ± 0.28	10.6 ± 3.0	7123.0 ± 0.3
	7113.68 ± 0.11		
Fe-Yfh1, S, and Isu1	7112.90 ± 0.28	16.2 ± 0.9	7123.0 ± 0.7
Fe(II) (aqueous)	7111.18 ± 0.07[c]	3.9 ± 0.3[c]	7122.9 ± 0.1[b]
	7112.03 ± 0.15[c]		
	7113.58 ± 0.03[c]		

[a]Pre-edge transition energies and areas determined using EDG_FIT. Edge inflection energies quantified as the maximum value of the calculated first derivative of the XAS edge feature. [b]See ref *21*. [c]See ref *48*.

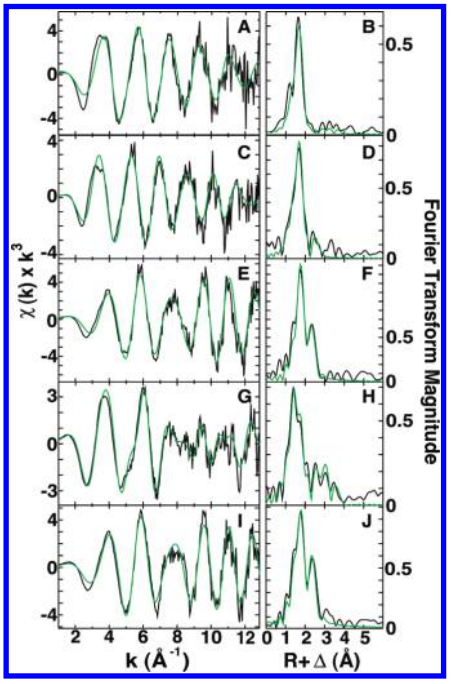

FIGURE 4: EXAFS and Fourier transforms of EXAFS data for iron at different stages of Fe−S cluster assembly. Raw EXAFS data in black for (A) Fe-Yfh1, (C) Fe-Isu1, (E) Fe-Isu1 and S^{2-}, (G) Fe-Yfh1 and Isu1, and (I) Fe-Yfh1, S^{2-}, and Isu1. Corresponding Fourier transform plots of raw EXAFS data in black for (B) Fe-Yfh1, (D) Fe-Isu1, (F) Fe-Isu1 and S^{2-}, (H) Fe-Yfh1 and Isu1, and (J) Fe-Yfh1, S^{2-}, and Isu1.

Table 3: Summary of the Best-Fit EXAFS Simulation Analysis for Iron at Multiple Stages during Fe−S Cluster Assembly[a]

	Fe nearest neighbor ligands[b]				Fe long-range ligands[b]				
sample	atom[c]	R (Å)[d]	CN[e]	σ^{2f} (×10³ Å²)	atom[c]	R (Å)[d]	CN[e]	σ^{2f} (×10³ Å²)	F[g]
Fe-Yfh1	O/N	2.12	5.0	5.80	C	3.07	2.0	4.30	0.98
					C	3.30	1.5	4.41	
Fe-Isu1	O/N	2.01	1.0	1.91	C	3.01	1.5	1.14	0.99
	O/N	2.14	4.5	3.25					
Fe-Isu1 and S	O/N	2.11	2.5	5.05	Fe	2.69	0.5	1.70	0.69
	S	2.26	1.0	2.45					
Fe-Yfh1 and Isu1	O/N	1.99	2.0	5.40	C	3.07	2.5	5.58	0.32
	O/N	2.15	1.5	1.50	C	3.51	2.0	1.91	
					C	4.09	1.5	1.80	
Fe-Yfh1, Isu1, and S	O/N	2.04	1.5	4.20	Fe	2.70	0.5	1.20	0.46
	S	2.28	1.0	1.88					

[a]Values reported are the average of at least two independent data sets. [b]Independent metal−ligand scattering environment. [c]Scattering atoms: O (oxygen), N (nitrogen), C (carbon), S (sulfur), and Fe (iron). [d]Metal−ligand bond length. [e]Metal−ligand coordination number. [f]Debye−Waller factor. [g]Number of degrees of freedom-weighted mean square deviation between data and fit.

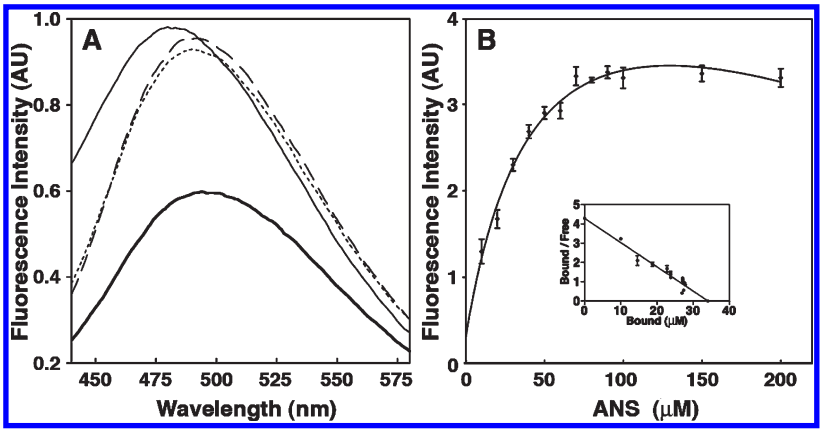

FIGURE 5: Characterization of the Isu1 fold using fluorescence spectroscopy. (A) Molten globule nature of Isu1 determined by fluorescence spectroscopy. Fluorescence of ANS bound to Isu1 alone (thin solid line), Isu1 incubated with Fe(II) (dashed line), Isu1 incubated with S^{2-} (dotted line), and Isu1 incubated with Fe(II) and then S^{2-} (thick solid line). (B) Fluorescence titration of Isu1 with ANS monitored at 476 nm. The inset shows the Scatchard analysis for the binding of ANS to Isu1.

atom at 2.26 Å, and a distinct Fe···Fe interaction at 2.69 Å, bond lengths consistent with a portion of the iron (<50%) being coordinated in a Fe−S cluster (*34*). Addition of sulfur to the Fe-Yfh1−Isu1 complex (Figure 4I,J) shifts the nearest neighbor metal−ligand environment to 1.5 O/N ligands centered at 2.04 Å, 1 S atom at 2.28 Å, and a distinct Fe···Fe interaction at 2.70 Å, again consistent with a portion of the metal (<50%) being coordinated in a Fe−S cluster. No long-range carbon scattering at $R > 3.0$ Å was detected in either sulfur-containing sample.

Fluorescence Spectroscopy. Fluorescence spectroscopy was used to characterize Isu1 structural changes coupled to iron or sulfide binding, or following Fe−S cluster formation. Binding of the fluorescent probe ANS is often used to characterize the globular nature of biomolecules, because ANS selectively binds to solvent-exposed hydrophobic regions in molten globule proteins. Binding induces a fluorescence signal in the vicinity of 500 nm ($\lambda_{excitation}$ = 371 nm), whereas well-folded proteins bind little dye and exhibit little fluorescence. Apo-Isu1 exposed to ANS exhibits a large fluorescence signal centered at 480 nm (Figure 5A, thin solid line). At these concentrations, ANS in buffer by itself had negligible fluorescence (control not shown). Reverse titration analysis of ANS into Isu1 indicated a maximum concentration of ligand bound to Isu1 (B_{max}) of 34.44 ± 0.49 μM. The dissociation constant (K_D) for the dissociation of ANS to Isu1, obtained from Scatchard analysis, was 7.73 ± 0.31 μM. The linear nature of the bound/free ANS versus free ANS from the Scatchard analysis (Figure 5B, inset) indicates a single ANS binding site on the protein.

The effect of structural changes on Isu1 coupled with Fe(II) or S^{2-} binding was also tested by fluorescence spectroscopy. Addition of either ferrous iron (Figure 5A, long dash line) or sulfide (Figure 5A, short dash line) to the Isu1/ANS mixture yields only subtle changes in fluorescence intensity, although the fluorescence maximum was red-shifted to 490 nm in both cases, indicating an increase in the polarity of the ANS binding environment coupled with substrate binding (*35*). Interestingly, incubation of both ferrous iron and sulfide to Isu1 prior to the addition of dye results in a substantial decrease in signal intensity (Figure 5A, thick solid line), suggesting a reduction in ANS accessibility to Isu1 (or an increase in the Isu1 fold) coupled to the formation of a complete Fe−S cluster.

DISCUSSION

Mounting evidence suggests that de novo Fe−S cluster assembly within the ISC pathway occurs via formation of a multiprotein complex consisting of the cysteine desulfurase, the assembly scaffold, frataxin, and, in eukaryotes, the accessory protein Isd11 (*4*, *36*). Here we provide molecular details of the interaction of frataxin with the scaffold protein, one event in multiprotein complex formation. In yeast, a direct interaction between Yfh1 and Isu1 is well-documented, confirming that binding can occur separately from multiprotein complex formation and suggesting that contact between these two partner partners may drive mutiprotein complex formation. Frataxin also interacts separately with the cysteine desulfurase and with Isd11, so future investigation of these interactions distinct from multiprotein complex formation is also certainly justified. Our goal is to dissect each protein−protein interaction separately, starting with the frataxin−scaffold protein interaction and then building toward a global understanding of structural changes that occur during multiprotein complex formation. Key differences between the prokaryotic and eukaryotic systems (for example, the presence of Isd11 in eukaryotes) indicate interactions between protein orthologs may be partially unique for the system under investigation, so clarification of these interactions within the yeast system may help explain key differences in the function of frataxin between different species (i.e., iron delivery or storage vs pathway regulation). In addition, this report follows the structural path of delivery of iron to Isu1 during multiple stages of Fe−S cluster assembly. In summary, we provide in this report the structural and thermodynamic details essential for understanding Fe−S cluster assembly at a molecular level, short of having the complete multiprotein complex structure.

Our NMR mapping results indicate that Yfh1 binds to Isu1 utilizing the frataxin α1−β1 acidic ridge and a large section of the β-sheet surface of the protein. Included in this binding region are the two Yfh1 iron binding sites previously identified by NMR (*21*). The overlap of these Yfh1 iron binding sites with the Isu1 interaction interface would be consistent with an iron delivery function for frataxin. The Yfh1 surface shown here to bind to Isu1 includes key residues shown to be essential for Fe−S cluster assembly. Others have shown substitution of conserved acidic residues (D86 and E89 on α1 or D101 and E103 on β1) by lysine impairs Fe−S cluster assembly, weakens the interaction between Yfh1 and Isu1, and increases the level of oxidative damage in the cell (*37*). Mutations of residues in the third β-strand region (either N122 itself or as a N122, K123, Q124 triple mutant) or at positions Q129, W131 (β4), and R141 (β5)

also show severe functional defects and decreased affinity of Yfh1 for Isu1 (*8*, *13*). Frataxin's α1−β1 acidic ridge has also been shown to participate in the bacterial frataxin binding surface for the cysteine desulfurase (*14*), so it seems possible that the cysteine desulfurase and scaffold bind contiguously to this region of frataxin.

Binding between Yfh1 and Isu1 is selective by nature (*8*, *13*, *38*, *39*). Yfh1 or Isu1 individually bind iron, but with different affinities, suggesting that energetic factors could be key determinants in the selective delivery of iron from Yfh1 to Isu1 if frataxin is serving as an iron chaperone. Binding affinities of iron for the different frataxin orthologs are all in the micromolar range (see ref *7* for a review), whereas binding affinities of iron for the different scaffold protein orthologs are generally submicromolar (*16*). Binding between Yfh1 and Isu1 is also iron-dependent. Interestingly, while Yfh1 binds two iron atoms, the binding site on Yfh1 is weaker than the tighter binding measured between holo-Yfh1 and Isu1. The presence of Nfs1 and Isd11 will surely alter these binding affinities, and experiments directed at measuring these additional binding interactions are currently underway. However, our results indicate that it would be energetically favorable for holo-Yfh1 and apo-Isu1 to interact in the presence of iron. This protein−protein binding would then allow the transfer of metal to Isu1 and following removal of metal from frataxin would cause the release of Yfh1 from Isu1.

Snapshots of the structural and electronic details of iron during the different stages in the Yfh1−Isu1 interaction provide insights into how metal is utilized during cluster assembly. Our data highlight, in the absence of sulfide, the possibility that iron exists in at least three stages, starting with its binding to Yfh1, then in the Yfh1−Isu1 complex, and ending with its binding to Isu1 alone. In all three states, iron is stable as high-spin six-coordinate Fe(II) coordinated by only oxygen- or nitrogen-based ligands. Analysis of the metric details of the metal−ligand structure indicates that the coordination environment of Fe(II) bound to Isu1 is distinct from that of Fe(II) on Yfh1 alone or in the Yfh1−Isu1 complex, suggesting that metal bound to Isu1 alone is the end point following delivery. Surprisingly, there is no evidence of sulfur ligation of iron bound to Isu1. Our data therefore suggest that when Isu1 initially binds iron, the protein utilizes a site distinct from the cysteine-rich assembly site.

Introduction of sulfide to iron bound-Isu1 (either in complex with Yfh1 or alone) induces the formation of a multinuclear Fe species structurally consistent with a [2Fe-2S] cluster. Shifts in the pre-edge feature and edge energy are consistent with a percentage of the iron (at a 50% lower limit) being shifted to a four-coordinate sulfur-containing structure. Metric parameters for Isu1-bound iron in this Fe−S structure indicate two iron atoms occur at ca. 2.7 Å, consistent with the formation of an authentic [2Fe-2S] cluster (*34*). In addition, these results are consistent with our recent spectroscopic characterization of the formation of a Fe−S cluster based on the 435 nm chromophore seen in the UV−vis assembly assay for Isu1 in the presence of both Fe and S (*15*).

The global fold of Isu1 becomes more defined as a result of Fe−S cluster formation. Structures of multiple IscU orthologs exhibit shared features, including the presence of an α−β core (*40*−*44*). In many cases, homogeneity in structure and the extent of the ortholog's fold are influenced by the presence of metal. ANS binding fluorescence was used to determine the molten globular nature of *Thermotoga maritima* IscU in solution (*45*). Our data indicate binding of Fe^{2+} or S^{2-} alone by Isu1 has only a minimal effect on the protein's fold, although a red shift seen in fluorescence is consistent with substrates influencing an increase in the molecule's global environmental polarity (*35*). Concurrent with or following Fe−S cluster formation, the Isu1 structure shifts to an increased fold with a hydrophobic core that better excludes solvent. This increase in fold is consistent with the well-folded *Aquifex aeolicus* IscU structure that was determined with a Fe−S cluster bound (*46*). It should be noted that our experiments were performed on the D37A Isu1 mutant to ensure retention of the bound Fe−S cluster; this mutant was selected so we could study Isu1 with an intact cluster. In the D37A Isu1 mutant, in the absence of the conserved aspartic acid, a conserved histidine preceding the most C-terminal cysteine is believed to supply the fourth ligand to the cluster (*47*), thereby locking the cluster in place. While there are certainly structural differences resulting from this mutation, we expect that the changes will be local relative to the overall protein fold because these residues are in a surface-exposed location. We would further expect that the wild-type Isu1 protein would release the cluster intermediate as part of a later step in Fe−S cluster assembly, subsequently returning to its initial flexible state. The increased flexibility obtained upon cofactor release would likely help prime Isu1 for the next round of cluster assembly.

Mounting evidence suggests that yeast mitochondrial Fe−S cluster assembly requires interactions between proteins forming a whole or subset of a Nfs1−Isd11−Isu1−Yfh1 multiprotein complex. Insight into the structure of this complex can be gained from studies of orthologous protein interactions. Structural details for the bacterial IscS−IscU complex have recently emerged, providing direct insight into how cysteine desulfurase and the scaffold interact (*44*). In the structure, IscU binds to the C-terminal region of IscS in the proximity of the cysteine desulfurase critical active site cysteine (Cys328). In the process, bound IscU projects its three conserved cysteine active site residues toward the IscS loop that carries Cys328. Interestingly, binding of IscU to IscS induces an increase in the fold of the N-terminal region of the scaffold protein. Mutagenesis studies of bacterial frataxin (CyaY) binding to IscS showed frataxin interacting with the cysteine desulfurase in a region in the proximity of but distinct from Cys328; binding of CyaY did not disrupt the transfer of sulfur from IscS to IscU. NMR chemical shift mapping studies showed CyaY interacting with IscS through multiple residues on frataxin's acidic (helix 1−strand 1) acidic ridge (*14*). Combined, these studies provide structural details for how IscU and IscS interact and for how IscS and CyaY interact. However, molecular details regarding frataxin's interaction with the scaffold protein remain ambiguous.

Our results, when combined with the structural details listed above, allow us to propose a structural model for how Yfh1 interacts with Isu1 during the initial stages of Fe−S cluster assembly. A large portion of frataxin's β-sheet surface, along with the N-terminal helix, forms the interface with Isu1, and this interaction is iron-dependent. This Isu1-interacting surface of frataxin encompasses the two Yfh1 iron binding sites. When utilized, this would position Yfh1 for iron delivery or for assisting in stabilization of the intermolecular interface. An interaction with the cysteine desulfurase residues in one of the Nfs1 monomers that participate in CyaY binding would position frataxin so it could interact with the second cysteine desulfurase monomer in the dimer; this would occur in the proximity of the scaffold protein binding site (*44*). By modeling the Isu1 and Nfs1 structures from the bacterial orthologs, we developed a model

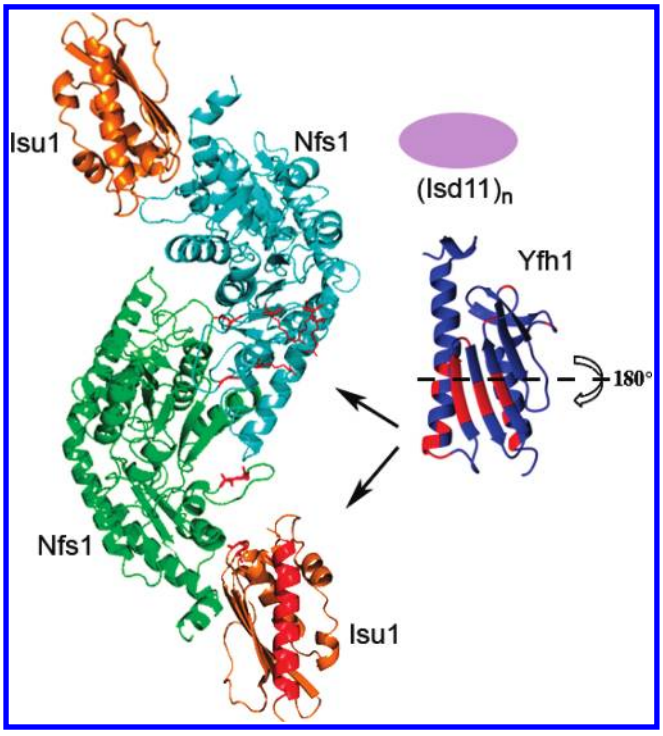

FIGURE 6: Model for the formation of the multiprotein complex required for Fe−S cluster assembly in the ISU pathway. The Isu1 and Nfs1 structures are modeled on the basis of the bacterial IscS/U structure (PDB entry 3LVL). Residues identified colored red on Nfs1 were identified as being essential to the binding of frataxin (*14*, *44*). Frataxin's Isu1 binding surface is displayed, but the protein must undergo a 180° horizontal axis rotation to fit in the binding pocket. Finally, while Isd11 is essential for in vivo Fe−S cluster assembly, structural details for the protein are lacking so the protein is shown as only an oval.

for how these three proteins could come together to perform cluster assembly (Figure 6). In our model, Yfh1 could bind to Isu1 and also possibly to Nfs1 in the active site regions using residues identified above to be involved in protein−protein interactions with only minimal distortion of the Isu1−Nfs1 protein complex structure (red residues in Figure 6). In our model, frataxin binding would require subtle movement of the Nfs1 dimer−Isu1 orientation, and this movement has already been proposed to bring cysteine desulfurase and the scaffold protein together (*44*). Structural details for frataxin's interaction with Isd11 are currently being sought, and while not included in detail in our model, the accessory protein could modify the movement of the Isu1−Nfs1 complex relative to frataxin's position by also binding in this region. Sulfur delivery for Fe−S cluster assembly may occur simultaneously with these protein interactions. In our model, iron is delivered to Isu1 using surface-exposed residues amenable for both frataxin binding and close to the Fe−S cluster assembly site. Following iron delivery, frataxin would dissociate from the multiprotein complex, prompting Isu1 to complete Fe−S cluster assembly. Structural and biochemical experiments are currently underway to test this model and to further characterize the individual interaction of frataxin with each additional binding partner.

ACKNOWLEDGMENT

Portions of this research were conducted at both the Stanford Synchrotron Radiation Laboratory (SSRL) and the National Synchrotron Light Source (NSLS). SSRL is a national user facility operated by Stanford University on behalf of the U.S. Department of Energy, Office of Basic Energy Sciences. The SSRL Structural Molecular Biology Program is supported by the Department of Energy, Office of Biological and Environmental Research, and by the National Institutes of Health, National Center for Research Resources, Biomedical Technology Program. NSLS, located at Brookhaven National Laboratory, is supported by the U.S. Department of Energy, Division of Materials Sciences and Division of Chemical Sciences, under Contract DE-AC02-98CH10886.

REFERENCES

1. Beinert, H., Holm, R. H., and Munck, E. (1997) Iron-sulfur clusters: Nature's modular, multipurpose structures. *Science 277*, 653–659.
2. Johnson, D. C., Dean, D. R., Smith, A. D., and Johnson, M. K. (2005) Structure, function, and formation of biological iron-sulfur clusters. *Annu. Rev. Biochem. 74*, 247–281.
3. Fontecave, M., and Ollagnier-de-Choudens, S. (2008) Iron-sulfur cluster biosynthesis in bacteria: Mechanisms of cluster assembly and transfer. *Arch. Biochem. Biophys. 474*, 226–237.
4. Lill, R. (2009) Function and biogenesis of iron-sulphur proteins. *Nature 460*, 831–838.
5. Gerber, J., Muhlenhoff, U., and Lill, R. (2003) An interaction between frataxin and Isu1/Nfs1 that is crucial for Fe/S cluster synthesis on Isu1. *EMBO Rep. 4*, 906–911.
6. Layer, G., Ollagnier-de Choudens, S., Sanakis, Y., and Fontecave, M. (2006) Iron-sulfur cluster biosynthesis: Characterization of *Escherichia coli* CYaY as an iron donor for the assembly of [2Fe-2S] clusters in the scaffold IscU. *J. Biol. Chem. 281*, 16256–16263.
7. Bencze, K. Z., Kondapalli, K. C., Cook, J. D., McMahon, S., Millan-Pacheco, C., Pastor, N., and Stemmler, T. L. (2006) The structure and function of frataxin. *Crit. Rev. Biochem. Mol. Biol. 41*, 269–291.
8. Wang, T., and Craig, E. A. (2008) Binding of yeast frataxin to the scaffold for Fe-S cluster biogenesis, Isu. *J. Biol. Chem. 283*, 12674–12679.
9. Campuzano, V., Montermini, L., Molto, M. D., Pianese, L., Cossee, M., Cavalcanti, F., Monros, E., Rodius, F., Duclos, F., Monticelli, A., Zara, F., Canizares, J., Koutnikova, H., Bidichandani, S. I., Gellera, C., Brice, A., Trouillas, P., De Michele, G., Filla, A., De Frutos, R., Palau, F., Patel, P. I., Di Donato, S., Mandel, J. L., Cocozza, S., Koenig, M., and Pandolfo, M. (1996) Friedreich's ataxia: Autosomal recessive disease caused by an intronic GAA triplet repeat expansion. *Science 271*, 1423–1427.
10. Babcock, M., de Silva, D., Oaks, R., Davis-Kaplan, S., Jiralerspong, S., Montermini, L., Pandolfo, M., and Kaplan, J. (1997) Regulation of mitochondrial iron accumulation by Yfh1p, a putative homolog of frataxin. *Science 276*, 1709–1712.
11. Rotig, A., de Lonlay, P., Chretien, D., Foury, F., Koenig, M., Sidi, D., Munnich, A., and Rustin, P. (1997) Aconitase and mitochondrial iron-sulphur protein deficiency in Friedreich ataxia. *Nat. Genet. 17*, 215–217.
12. Huang, M. L., Becker, E. M., Whitnall, M., Rahmanto, Y. S., Ponka, P., and Richardson, D. R. (2009) Elucidation of the mechanism of mitochondrial iron loading in Friedreich's ataxia by analysis of a mouse mutant. *Proc. Natl. Acad. Sci. U.S.A. 106*, 16381–16386.
13. Leidgens, S., De Smet, S., and Foury, F. (2010) Frataxin interacts with Isu1 through a conserved tryptophan in its β-sheet. *Hum. Mol. Genet. 19*, 276–286.
14. Adinolfi, S., Iannuzzi, C., Prischi, F., Pastore, C., Iametti, S., Martin, S. R., Bonomi, F., and Pastore, A. (2009) Bacterial frataxin CyaY is the gatekeeper of iron-sulfur cluster formation catalyzed by IscS. *Nat. Struct. Mol. Biol. 16*, 390–396.
15. Kondapalli, K. C., Kok, N. M., Dancis, A., and Stemmler, T. L. (2008) *Drosophila* frataxin: An iron chaperone during cellular Fe-S cluster bioassembly. *Biochemistry 47*, 6917–6927.
16. Yoon, T., and Cowan, J. A. (2003) Iron-sulfur cluster biosynthesis. Characterization of frataxin as an iron donor for assembly of [2Fe-2S] clusters in ISU-type proteins. *J. Am. Chem. Soc. 125*, 6078–6084.
17. Adamec, J., Rusnak, F., Owen, W. G., Naylor, S., Benson, L. M., Gacy, A. M., and Isaya, G. (2000) Iron-dependent self-assembly of recombinant yeast frataxin: Implications for Friedreich ataxia. *Am. J. Hum. Genet. 67*, 549–562.
18. Gakh, O., Adamec, J., Gacy, A. M., Twesten, R. D., Owen, W. G., and Isaya, G. (2002) Physical evidence that yeast frataxin is an iron storage protein. *Biochemistry 41*, 6798–6804.

19. Aloria, K., Schilke, B., Andrew, A., and Craig, E. A. (2004) Iron-induced oligomerization of yeast frataxin homologue Yfh1 is dispensable in vivo. *EMBO Rep. 5*, 1096–1101.
20. Bou-Abdallah, F., Adinolfi, S., Pastore, A., Laue, T. M., and Dennis Chasteen, N. (2004) Iron binding and oxidation kinetics in frataxin CyaY of *Escherichia coli*. *J. Mol. Biol. 341*, 605–615.
21. Cook, J. D., Bencze, K. Z., Jankovic, A. D., Crater, A. K., Busch, C. N., Bradley, P. B., Stemmler, A. J., Spaller, M. R., and Stemmler, T. L. (2006) Monomeric yeast frataxin is an iron-binding protein. *Biochemistry 45*, 7767–7777.
22. He, Y., Alam, S. L., Proteasa, S. V., Zhang, Y., Lesuisse, E., Dancis, A., and Stemmler, T. L. (2004) Yeast frataxin solution structure, iron binding, and ferrochelatase interaction. *Biochemistry 43*, 16254–16262.
23. Nair, M., Adinolfi, S., Pastore, C., Kelly, G., Temussi, P., and Pastore, A. (2004) Solution structure of the bacterial frataxin ortholog, CyaY: Mapping the iron binding sites. *Structure 12*, 2037–2048.
24. Huang, J., Dizin, E., and Cowan, J. A. (2008) Mapping iron binding sites on human frataxin: Implications for cluster assembly on the ISU Fe-S cluster scaffold protein. *J. Biol. Inorg. Chem. 13*, 825–836.
25. Studier, F. W. (2005) Protein production by auto-induction in high density shaking cultures. *Protein Expression Purif. 41*, 207–234.
26. Pervushin, K., Braun, D., Fernandez, C., and Wuthrich, K. (2000) [^{15}N,^{1}H]/[^{13}C,^{1}H]-TROSY for simultaneous detection of backbone ^{15}N-^{1}H, aromatic ^{13}C-^{1}H and side-chain ^{15}N-^{1}H$_2$ correlations in large proteins. *J. Biomol. NMR 17*, 195–202.
27. Delaglio, F., Grzesiek, S., Vuister, G. W., Zhu, G., Pfeifer, J., and Bax, A. (1995) NMRPipe: A multidimensional spectral processing system based on UNIX pipes. *J. Biomol. NMR 6*, 277–293.
28. Goddard, T. D., and Kneller, D. G. (2001) SPARKY 3, University of California, San Francisco.
29. George, G. N., George, S. J., and Pickering, I. J. (2001) EXAFSPAK, Stanford Synchrotron Radiation Laboratory, Menlo Park, CA. http://www-ssrl.slac.stanford.edu/~george/exafspak/exafs.htm.
30. Bencze, K. Z., Kondapalli, K. C., and Stemmler, T. L. (2007) X-Ray Absorption Spectroscopy. In Applications of Physical Methods in Inorganic and Bioinorganic Chemistry: Handbook, Encyclopedia of Inorganic Chemistry (Scott, R. A., and Lukehart, C. M., Eds.) 2nd ed., pp 513−528, John Wiley & Sons, Ltd., Chichester, U.K.
31. Semisotnov, G. V., Rodionova, N. A., Razgulyaev, O. I., Uversky, V. N., Gripas, A. F., and Gilmanshin, R. I. (1991) Study of the "molten globule" intermediate state in protein folding by a hydrophobic fluorescent probe. *Biopolymers 31*, 119–128.
32. Reddy, G. B., Das, K. P., Petrash, J. M., and Surewicz, W. K. (2000) Temperature-dependent chaperone activity and structural properties of human αA- and αB-crystallins. *J. Biol. Chem. 275*, 4565–4570.
33. Roe, A. L., Schneider, D. J., Mayer, R. L., Pyrz, J. W., Widon, J., and Que, L., Jr. (1984) X-ray absorption spectroscopy of iron-tyrosinate proteins. *J. Am. Chem. Soc. 106*, 1676–1681.
34. Sazinsky, M. H., LeMoine, B., Orofino, M., Davydov, R., Bencze, K. Z., Stemmler, T. L., Hoffman, B. M., Arguello, J. M., and Rosenzweig, A. C. (2007) Characterization and structure of a Zn^{2+} and [2Fe-2S]-containing copper chaperone from *Archaeoglobus fulgidus*. *J. Biol. Chem. 282*, 25950–25959.
35. Hawe, A., Sutter, M., and Jiskoot, W. (2008) Extrinsic fluorescent dyes as tools for protein characterization. *Pharm. Res. 25*, 1487–1499.
36. Raulfs, E. C., O'Carroll, I. P., Dos Santos, P. C., Unciuleac, M. C., and Dean, D. R. (2008) In vivo iron-sulfur cluster formation. *Proc. Natl. Acad. Sci. U.S.A. 105*, 8591–8596.
37. Foury, F., Pastore, A., and Trincal, M. (2007) Acidic residues of yeast frataxin have an essential role in Fe-S cluster assembly. *EMBO Rep. 8*, 194–199.
38. Ramazzotti, A., Vanmansart, V., and Foury, F. (2004) Mitochondrial functional interactions between frataxin and Isu1p, the iron-sulfur cluster scaffold protein, in *Saccharomyces cerevisiae*. *FEBS Lett. 557*, 215–220.
39. Li, H., Gakh, O., Smith, D. Y., IV, and Isaya, G. (2009) Oligomeric yeast frataxin drives assembly of core machinery for mitochondrial iron-sulfur cluster synthesis. *J. Biol. Chem. 284*, 21971–21980.
40. Bertini, I., Cowan, J. A., Del Bianco, C., Luchinat, C., and Mansy, S. S. (2003) *Thermotoga maritima* IscU. Structural characterization and dynamics of a new class of metallochaperone. *J. Mol. Biol. 331*, 907–924.
41. Ramelot, T. A., Cort, J. R., Goldsmith-Fischman, S., Kornhaber, G. J., Xiao, R., Shastry, R., Acton, T. B., Honig, B., Montelione, G. T., and Kennedy, M. A. (2004) Solution NMR structure of the iron-sulfur cluster assembly protein U (IscU) with zinc bound at the active site. *J. Mol. Biol. 344*, 567–583.
42. Adinolfi, S., Rizzo, F., Masino, L., Nair, M., Martin, S. R., Pastore, A., and Temussi, P. A. (2004) Bacterial IscU is a well folded and functional single domain protein. *Eur. J. Biochem. 271*, 2093–2100.
43. Liu, J., Oganesyan, N., Shin, D. H., Jancarik, J., Yokota, H., Kim, R., and Kim, S. H. (2005) Structural characterization of an iron-sulfur cluster assembly protein IscU in a zinc-bound form. *Proteins 59*, 875–881.
44. Shi, R., Proteau, A., Villarroya, M., Moukadiri, I., Zhang, L., Trempe, J. F., Matte, A., Armengod, M. E., and Cygler, M. (2010) Structural basis for Fe-S cluster assembly and tRNA thiolation mediated by IscS protein-protein interactions. *PLoS Biol. 8*, 1–18.
45. Mansy, S. S., and Cowan, J. A. (2004) Iron-sulfur cluster biosynthesis: Toward an understanding of cellular machinery and molecular mechanism. *Acc. Chem. Res. 37*, 719–725.
46. Shimomura, Y., Wada, K., Fukuyama, K., and Takahashi, Y. (2008) The asymmetric trimeric architecture of [2Fe-2S] IscU: Implications for its scaffolding during iron-sulfur cluster biosynthesis. *J. Mol. Biol. 383*, 133–143.
47. Bandyopadhyay, S., Chandramouli, K., and Johnson, M. K. (2008) Iron-sulfur cluster biosynthesis. *Biochem. Soc. Trans. 36*, 1112–1119.
48. Westre, T. E., Kennepohl, P., DeWitt, J. G., Hedman, B., Hodgson, K. O., and Solomon, E. I. (1997) A Multiplet Analysis of the Fe K-Edge 1s → 3d Pre-Edge Features of Iron Complexes. *J. Am. Chem. Soc. 119*, 6297–6314.